

Time resolved photoemission of Sr_2IrO_4

C. Piovera¹, V. Brouet², E. Papalazarou², M. Caputo², M. Marsi², A. Taleb-Ibrahimi³, B. J. Kim⁴, and L. Perfetti¹

¹ Laboratoire des Solides Irradiés, Ecole Polytechnique, CNRS,
CEA, Université Paris-Saclay, 91128 Palaiseau, France

² Laboratoire de Physique des Solides, CNRS, Univ. Paris-Sud,
Université Paris-Saclay, 91405 Orsay Cedex, France

³ Synchrotron SOLEIL, L'Orme des Merisiers, Saint-Aubin-BP 48, F-91192 Gif sur Yvette, France and

⁴ Max Planck Institute for Solid State Research, Heisenbergstrae 1, D-70569 Stuttgart, Germany

(Dated: December 3, 2024)

We investigate the temporal evolution of electronic states in strontium iridate Sr_2IrO_4 . The time resolved photoemission spectra of intrinsic, electron doped and the hole doped samples are monitored in identical experimental conditions. Our data on intrinsic and electron doped samples, show that primary doublon-holon pairs relax near to the chemical potential on a timescale shorter than 70 fs. The subsequent cooling of low energy excitations takes place in two step: a rapid dynamics of $\cong 120$ fs is followed by a slower decay of $\cong 1$ ps. The reported timescales endorse the analogies between Sr_2IrO_4 and copper oxides.

PACS numbers: 73.20.Mf, 71.15.Mb, 73.20.At, 78.47.jb

The layered Sr_2IrO_4 is an ideal system where to explore electronic correlations, electron-phonon coupling and antiferromagnetic ordering. Strontium iridate is a quasi-two-dimensional compound with partially filled 5d shell and moderate Coulomb repulsion. In spite of the large extension of 5d orbitals, the subtle interplay of spin-orbit interaction, crystal field splitting and antiferromagnetic interaction leads to an insulating state^{1,2}. Due to super-exchange interaction, the groundstate of Sr_2IrO_4 holds canted antiferromagnetic ordering of the spins on a squared lattice³. As in the case of copper oxides⁴, the paramagnetic insulator can be viewed as intermediate Mott-Slater system that is stabilized by short-range correlations of the antiferromagnetic order⁵. The analogy with cuprates can be pushed further^{6,7}, insofar as doped Sr_2IrO_4 is considered a promising candidate where to observe high temperature superconductivity⁸.

It is worth questioning whether iridates and cuprates display the same dynamical behavior upon photoexcitation. In this respect, the insulating copper oxides have already been characterized by exhaustive experiments of transient absorption⁹. H. Okamoto *et al.* measured at different probing frequencies, thereby disentangling the Drude component from the mid-gap response. It follows that mid-gap states arise on a timescale of 40 fs and experience an initial decay within 200 fs. The iridates seem to display a similar response, although the reported experiments have been performed with probing energy exceeding the optical gap value^{10,11}. D. Hsieh *et al.* observed a biexponential kinetic and analyzed the effects of the magnetic transition on the relaxation time¹⁰.

The purpose of this work is to directly follow the relaxation of electronic states in Sr_2IrO_4 . We report a time resolved photoemission experiment of the intrinsic and chemically doped samples. Our data indicate that primary doublon holon pairs are highly unstable against the formation of mid-gap states. The dynamics of such secondary excitations follow a biexponential law

that is compatible to the transient absorption reported in La_2CuO_4 ⁹. Our results provide further insights on the electron dynamics of Mott insulators and reinforce the analogies between iridates and cuprates.

Methods: Samples have been synthesized by a self flux method³. Electron doping is obtained by substituting 3% of the Sr atoms with La, whereas hole doping is done by replacing 15% of Sr atoms with Rh. The crystals have been characterized by X-ray diffraction, resistivity, magnetization measurements and angle resolved photo-electron spectroscopy. Time resolved photoemission experiments were performed on the FemtoARPES setup¹², using a Ti:sapphire laser system delivering 35 fs pulses at 780 nm with 250 kHz repetition rate. Part of the laser beam is used to generate a UV probe pulse for photoemission. The 6.3 eV photons are obtained through cascade frequency mixing in BBO crystals. The energy resolution is $\cong 60$ meV (limited by the energy bandwidth of the UV pulses) and the temporal resolution is $\cong 60$ fs. All the time resolved photomission measurements were performed at room temperature and at the base pressure of 7×10^{-11} mbars.

Samples Characterization: Figure 1(a,b) show examples of the resistivity and magnetization measurements in three different samples. The intrinsic Sr_2IrO_4 exhibits an insulating behavior with an activation energy of 30-70 meV. Upon chemical doping, the conductivity drops by two orders of magnitude. The magnetic phase transition is barely visible at electron-doping (3% La) and it vanishes at hole-doping (15% Rh).

According to the literature, the lower Hubbard band has orbital character $J_{eff} = 1/2$ and reaches the nearest distance from the chemical potential at the X point of the Brillouin zone^{1,13}. As shown in Fig. 1(c) the Hubbard peak is at $\cong -0.25$ eV in the intrinsic sample and shifts to $\cong -0.6$ eV after La substitution¹³. Upon hole doping (15% Rh), the peak of the $J_{eff} = 1/2$ band moves at $\cong -0.1$ eV from the chemical potential, giving rise to a

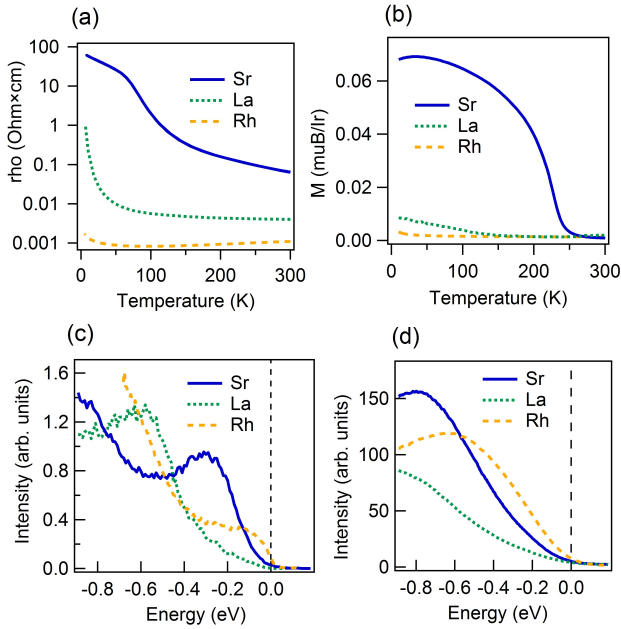


FIG. 1: In plane resistivity (a) and magnetization curves (b) of intrinsic and doped Sr_2IrO_4 . Angle resolved photoelectron spectra acquired at the X point of the Brillouin zone with photon energy of 70 eV (c) and acquired at center of the Brillouin zone with photon energy of 6 eV (d). The intrinsic (solid line), electron-doped (dotted line) and hole-doped (dashed line) compound are marked by the notations Sr, La and Rh, respectively.

small pseudogap instead of a quasiparticle crossing. We estimate a Mott gap of $\cong 0.6$ eV from the difference of the $J_{eff} = 1/2$ position in hole doped and electron doped compound¹³. This value is consistent with Scanning Tunneling Spectroscopy (STS) measurements on sample regions with no defects^{14,15}. The presence of defects is an unavoidable complexity that has strong impact on the low energy physics of iridates^{13–16}. STS experiments confirmed that defects induce a local collapse of the Mott gap¹⁴ and established a relation between mid-gap states and oxygen impurities¹⁵.

Finally, we show in Fig. 1(d) the spectra acquired with 6 eV photon energy at the center of the Brillouin zone and normalized to the photon flux. In the intrinsic sample, the direct photoemission from the $J_{eff} = 1/2$ band and the weak unklapp of the $J_{eff} = 3/2$ band should peak at 1.2 eV and 0.5 eV respectively^{1,13}. However, the signal in Fig. 1(d) mainly arises from photoelectronic emission assisted by surface roughness and phonons. It is reasonable to assume that these energy distribution curves provide a rough indication of the electron-removal spectral function integrated over the wavevector index. In agreement with Fig. 1(c), we observe a large shift of spectral weight due to electron or hole doping.

Properties of the photoexcited state: Figure 2 reports the pump-on minus pump-off spectra acquired on differ-

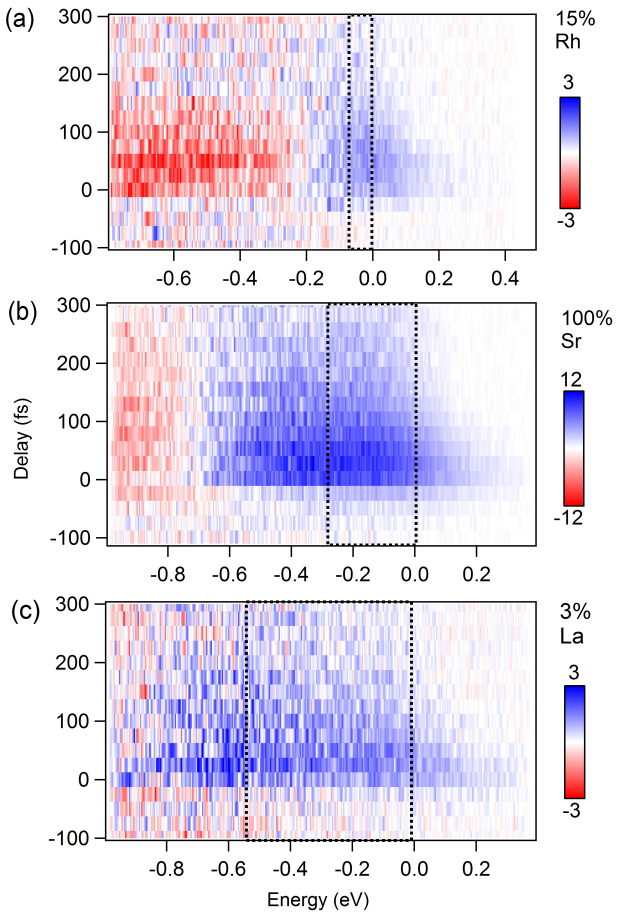


FIG. 2: Map of the pump-on minus pump-off signal acquired with 6 eV photons as a function of energy and pump-probe delay. The intensity is normalized with respect to the photon flux and the pump fluence has been set to $\cong 0.7$ mJ/cm². Data on Rh substituted, intrinsic and La substituted sample are shown in panel (a), (b) and (c) respectively. The dotted rectangles stand for the energy window comprised between the lower Hubbard band and the chemical potential.

ent samples as a function of delay time. The differential intensity is plotted on a colorscale where red and blue stand for photoinduced reduction and increase of photoelectron yield, respectively. Intensity map of Fig. 2(a), 2(b) and 2(c) have been acquired on Rh-substituted, intrinsic and La-substituted compound. We employed a pumping fluence of 0.7mJ/cm², leading to ~ 0.04 excitations per iridium atom. The data suggest that photoexcited electrons do not accumulate in the upper Hubbard band but relax in electronic states near to chemical potential. This finding is in contrast to recent time resolved photoemission measurements of the Mott insulator UO_2 ¹⁷. We propose two possible scenarios to explain the observed discrepancy. First, the Sr_2IrO_4 has a Mott gap (0.6 eV) much smaller than the one of UO_2 (2.3 eV)¹⁷. Therefore the rate of multi-phonon and multi-

magnon emission^{18,19} could be strong enough to relax electrons across the correlation gap of Sr_2IrO_4 whereas it may be negligible in UO_2 . Second, we know from STS data^{14,15} that defects locally disrupt the narrow Mott gap of Sr_2IrO_4 . As a consequence, the excited electrons may find viable paths to relax from the upper Hubbard band down to lower lying energies.

We outline in Fig. 2(a-c) that a photoinduced increase of photoemission yield extends well below the chemical potential. A combination of intrinsic and extrinsic effects can explain this finding. On one hand, an intrinsic increase of spectral weight between the lower Hubbard band and the chemical potential (dotted rectangles in Fig. 2) is expected because of the partial filling of the Mott gap. This behavior has been observed in 1T-TaS₂ at comparable excitation densities and should be a general property of Mott insulators with narrow gap^{20,21}. On the other hand, an extrinsic and time dependent shift of the spectrum can arise from the sudden change of dielectric properties at the surface of the sample. We already observed spectral shift generated by local fields in copper oxides²², small gap semiconductors²³ and semimetals²⁴. As in the case of surface photovoltage, we expect the energy displacement to be more important in the intrinsic compound than in samples with Rh or La substitutions. Future experiments with high harmonic sources^{17,25} could access the X point of the Brillouin zone and may shed light on this issue.

Dynamics of the electrons: Figure 3(a) shows pump-on minus pump-off spectra acquired in the intrinsic sample, at delay time of 25 fs and different pumping fluences. The spectra have similar shape and are nearly proportional to the pumping fluence. Therefore, the photoexcited state is still far from the saturation regime of a collapsed Mott insulator²¹.

We show in Fig. 3(b) the pump-on minus pump-off spectra of the intrinsic sample acquired with excitation fluence of 0.7 mJ/cm² at different pump-probe delays. Notice that electrons at excitation energy higher than ≈ 0.1 eV follow an exponential distribution $\exp(-\epsilon/kT_e)$ with temperature scale T_e attaining a maximal value of 1900 K. In order to gain further insights of the electronic relaxation, we plot in Fig. 3(c) the temporal evolution of the signal integrated in the energy interval [0.1,0.2] eV. A fit accounting for the cross-correlation between pump and probe beam provides the decay time $\tau_1 \approx 70$ fs. This timescale does not change with respect to photoexcitation density and indicates that primary doublon-holons pairs relax near the chemical potential on a very short timescale. Our results are in line with the sudden decay of the Drude response observed by Okamoto *et al.* in photoexcited cuprates⁹.

Next we turn on the temporal evolution of the pump-probe signal in the spectral region where mid-gap states accumulate. We cannot resolve any finite rise time in the pump-probe signal, indicating that mid-gap states are formed within less than 60 fs. Figure 3(d) shows the evolution of the photoelectron intensity integrated in the

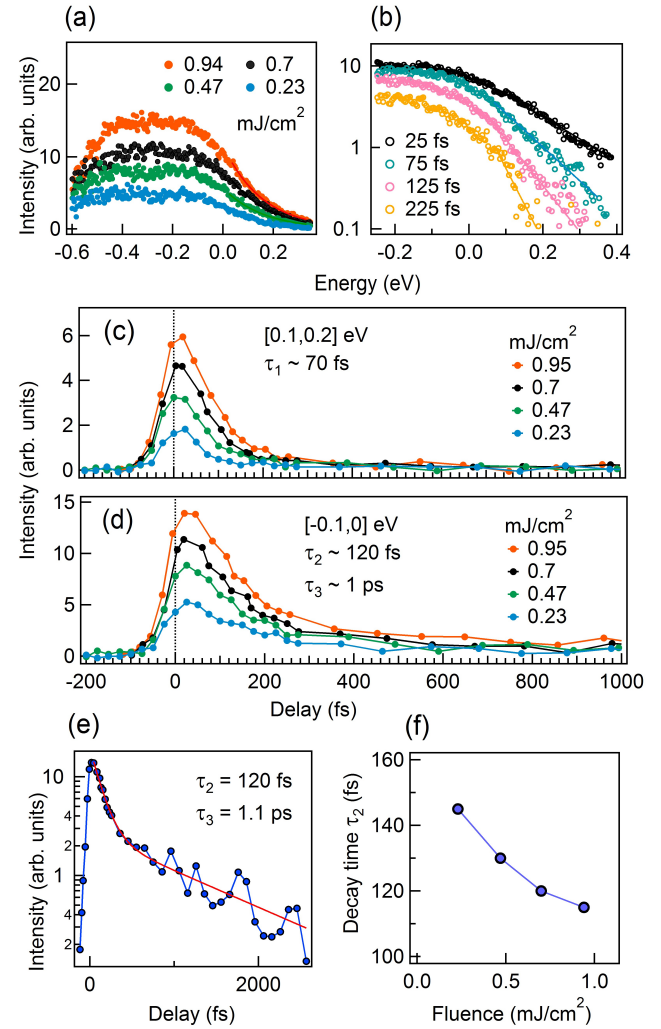


FIG. 3: All data of this figure refer to the intrinsic sample. (a) Energy distribution of the pump-on minus pump-off signal acquired at delay time of 25 fs at different pumping fluence. (b) Energy distribution of the pump-on minus pump of signal acquired with 0.7 mJ/cm² at different pump-probe delays. The solid lines stands for the exponential fit of the spectral tail at energy ≥ 0.1 eV. Evolution of the signal integrated in the energy interval [0.1, 0.2] eV (panel (c)) and [-0.1, 0] (panel (d)) as a function of delay time and for different fluences. e) Logarithmic plot of the [-0.1, 0] eV signal for pump fluence of 0.7 mJ/cm². f) Dependence of the decay time τ_2 on the pump fluence.

spectral range $[-0.1, 0]$ eV. The relaxation of the mid-gap signal follows a biexponential decay with time constant $\tau_2 \approx 120$ fs and $\tau_3 \approx 1$ ps. As shown in Fig. 3(e)), the presence of the two timescales is clearly resolved by plotting the decay curve on a logarithmic scale. Similar dynamics have been also reported in experiments of transient reflectivity at 1.5 eV¹⁰. Most importantly, we outline here the clear analogy between iridates and cuprates. According to Okamoto *et al.*, the midgap states of pho-

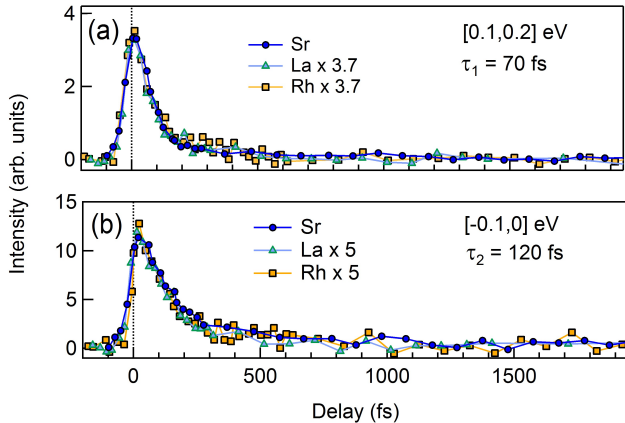


FIG. 4: Evolution of the pump-probe signal integrated in the energy interval $[0.1, 0.2]$ eV (panel (a)) and $[-0.1, 0]$ (panel (b)). The circles, triangles and squares stand for the intrinsic, La substituted and Rh substituted sample.

to excited La_2CuO_4 display an initial relaxation taking place within 200 fs⁹. Such fast recovery of the charge gap is typical of Mott insulators, whereas does not take place in correlated insulators where the partial gap filling comes along with large structural distortions^{27,28}.

As in the case of cuprates^{9,22,26}, we ascribe the τ_2 decay to the energy dissipation via emission of optical phonons or localized vibrations. The slower dynamics τ_3 is instead due to anharmonicity and acoustic phonon emission. Within our experimental accuracy we could

not observe any fluence dependence in the slow timescale τ_3 . Conversely, Fig. 3(f) shows a weak increase of τ_2 by lowering the photoexcitation density. At last, Fig. 4 compares the dynamics of the signal acquired on the intrinsic, Rh-substituted and La-substituted sample. Strikingly, we observe an identical temporal behavior in the three different samples. Independently on the doping, the excited electrons integrated in the interval $[0.1, 0.2]$ eV decay with time constant $\tau_1 = 70$ fs. Instead, the midgap states in the energy window $[-0.1, 0]$ eV follow a biexponential decay with time constants $\tau_2 = 120$ fs and $\tau_3 = 1.1$ ps.

In conclusion, time resolved photoemission measurements of Sr_2IrO_4 reveal the electrons dynamics upon photoexcitation above bandgap. The primary holon-doublon pairs decay in to midgap states on an ultrafast timescale. Presumably, this behavior arises from emission of collective excitations and defect mediated decay. We report identical dynamics in intrinsic and doped compounds, suggesting that metallicity and screening do not influence the relaxation of the photoexcited electrons. Our time resolved photoemission data of iridates are in good agreement with optical experiments on copper oxides, providing compelling evidence of common dynamics in these intermediate Mott-Slater insulators.

We acknowledge Silke Biermann, M. Ferrero and Martin Eckstein for enlightening discussions on the physics of Mott insulators and Iridates. This work is supported by Investissements d'Avenir LabEx PALM (grant No. ANR-10-LABX-0039PALM), by the EU/FP7 under the contract Go Fast (Grant No. 280555), and by the Région Ile-de-France through the program DIM OxyMORE.

¹ B. J. Kim, Hosub Jin, S. J. Moon, J.-Y. Kim, B.-G. Park, C. S. Leem, Jaejun Yu, T.W. Noh, C. Kim, S.-J. Oh, J.-H. Park, V. Durairaj, G. Cao, and E. Rotenberg, Phys. Rev. Lett. **101**, 076402 (2008).

² Cyril Martins, Markus Aichhorn, Log Vaugier, and Silke Biermann, Phys. Rev. Lett. **107**, 266404 (2011).

³ B. J. Kim, H. Ohsumi, T. Komesu, S. Sakai, T. Morita, H. Takagi, and T. Arima, Science **323**, 1329 (2009).

⁴ A. Comanac, L. de Medici, M. Capone and A. J. Millis, Nature Phys. **4**, 287 (2008).

⁵ H. Watanabe, T. Shirakawa, and S. Yunoki, Phys. Rev B **89**, 165115 (2014).

⁶ Y. K. Kim, O. Krupin, J. D. Denlinger, A. Bostwick, E. Rotenberg, Q. Zhao, J. F. Mitchell, J. W. Allen, B. J. Kim, Science **345**, 187 (2014).

⁷ A. de la Torre, S. McKeown Walker, F. Y. Bruno, S. Riccò, Z. Wang, I. Gutierrez Lezama, G. Scheerer, G. Giriati, D. Jaccard, C. Berthod, T. K. Kim, M. Hoesch, E. C. Hunter, R. S. Perry, A. Tamai, and F. Baumberger, Phys. Rev. Lett. **115**, 176402 (2015).

⁸ Y. K. Kim, N. H. Sung, J. D. Denlinger and B. J. Kim, Nature Physics **12**, 37 (2016).

⁹ H. Okamoto, T. Miyagoe, K. Kobayashi, H. Uemura, H. Nishioka, H. Matsuzaki, A. Sawa, and Y. Tokura, Phys. Rev. B **83**, 125102 (2011).

¹⁰ D. Hsieh, F. Mahmood, D. H. Torchinsky, G. Cao, and N. Gedik, Phys. Rev. B **86**, 035128 (2012).

¹¹ Z. Alpichshev, F. Mahmood, G. Cao and N. Gedik, Phys. Rev. Lett. **114**, 017203 (2015).

¹² J. Faure, J. Mauchain, E. Papalazarou, W. Yan, J. Pinon, M. Marsi, and L. Perfetti, Rev. Sci. Inst. **83**, 043109 (2012).

¹³ V. Brouet, J. Mansart, L. Perfetti, C. Piovera, I. Vobornik, P. Le Fèvre, F. Bertran, S. C. Riggs, M. C. Shapiro, P. Giraldo-Gallo, and I. R. Fisher, Phys. Rev. B **92**, 081117(R) (2015).

¹⁴ Y. Okada, D. Walkup, H. Lin, C. Dhital, T.-R. Chang, S. Khadka, W. Zhou, H.-T. Jeng, M. Paranjape, A. Bansil, Z. Wang, S. D. Wilson and V. Madhavan, Nature materials **12**, 707 (2013).

¹⁵ J. Dai, E. Calleja, G. Cao, and K. McElroy, Phys. Rev. B **90**, 041102 (2014).

¹⁶ A. Glamazda, W.-J. Lee, K.-Y. Choi, P. Lemmens, H. Y. Choi, N. Lee, and Y. J. Choi, Phys. Rev. B **89**, 104406

(2014).

¹⁷ S. M. Gilbertson, T. Durakiewicz, G. L. Dakovski, Y. Li, J.-X. Zhu, S. D. Conradson, S. A. Trugman, and G. Rodriguez, Phys. Rev. Lett. **112**, 087402 (2014).

¹⁸ Z. Lenarcic and P. Prelovsek, Phys. Rev. B **90**, 235136 (2014).

¹⁹ Z. Lenarcic, M. Eckstein, and P. Prelovsek, Phys. Rev. B **92**, 201104(R) (2015).

²⁰ L. Perfetti, P. A. Loukakos, M. Lisowski, U. Bovensiepen, H. Berger, S. Biermann, P. S. Cornaglia, A. Georges, and M. Wolf, Phys. Rev. Lett. **97**, 067402 (2006).

²¹ L. Perfetti, P. A. Loukakos, M. Lisowski, U. Bovensiepen, H. Berger, S. Biermann, A. Georges, and M. Wolf, New Journal of Physics **10**, 053019, (2008).

²² C. Piovera, Z. Zhang, M. d'Astuto, A. Taleb-Ibrahimi, E. Papalazarou, M. Marsi, Z. Z. Li, H. Raffy, and L. Perfetti, Phys. Rev. B **91**, 224509 (2015).

²³ J. Mauchain, Y. Ohtsubo, M. Hajlaoui, E. Papalazarou, M. Marsi, A. Taleb-Ibrahimi, J. Faure, K. A. Kokh, O. E. Tereshchenko, S. V. Eremeev, E. V. Chulkov, and L. Perfetti, Phys. Rev. Lett. **111**, 126603 (2013).

²⁴ E. Papalazarou, J. Faure, J. Mauchain, M. Marsi, A. Taleb-Ibrahimi, I. Reshetnyak, A. van Roekeghem, I. Timrov, N. Vast, B. Arnaud, and L. Perfetti, Phys. Rev. Lett. **108**, 256808 (2012).

²⁵ S. Hellmann, T. Rohwer, M. Kallie, K. Hanff, C. Sohrt, A. Stange, A. Carr, M. M. Murnane, H. C. Kapteyn, L. Kipp, M. Bauer and K. Rossnagel, Nature Comm. **3**, 1069 (2012).

²⁶ L. Perfetti, P. A. Loukakos, M. Lisowski, U. Bovensiepen, H. Eisaki, and M. Wolf, Phys. Rev. Lett. **99**, 197001(2007).

²⁷ V. Brouet, J. Mauchain, E. Papalazarou, J. Faure, M. Marsi, P. H. Lin, A. Taleb-Ibrahimi, P. Le Fèvre, F. Bertran, L. Cario, E. Janod, B. Corraze, V. T. Phuoc, and L. Perfetti, Phys. Rev. B **87**, 041106(R) (2013).

²⁸ R. Yoshida, T. Yamamoto, Y. Ishida, H. Nagao, T. Otsuka, K. Saeki, Y. Muraoka, R. Eguchi, K. Ishizaka, T. Kiss, S. Watanabe, T. Kanai, J. Itatani, and S. Shin, Phys. Rev. B **89**, 205114 (2014).